Efficient Single Photon Emission and Collection Based on Excitation of Gap Surface Plasmons

Hang Lian,[1] Ying Gu,[1,2,*] Juanjuan Ren,[1] Fan Zhang,[1] Luojia Wang,[1] and Qihuang Gong[1,2]
[1]State Key Laboratory for Mesoscopic Physics, Department of Physics, Peking University, Beijing 100871, China
[2]Collaborative Innovation Center of Quantum Matter, Beijing 100871, China
(Received 30 September 2014; published 15 May 2015)

Combining the advantages of ultrahigh photon emission rates achievable in the gap surface plasmon polaritons with high extraction decay rates into low-loss nanofibers, we demonstrate theoretically the efficient photon emission of a single dipole emitter and one-dimensional nanoscale guiding in metallic nanorod-coupled nanofilm structures coupled to dielectric nanofibers. We find that total decay rates and surface plasmon polariton channel decay rates orders of magnitude larger than those characteristic of metallic nanofilms alone can be achieved in ultrastrong hot spots of gap plasmons. For the requirement of practical applications, propagating single photons with decay rates of $290\gamma_0$–$770\gamma_0$ are guided into the phase-matched low-loss nanofibers. The proposed mechanism promises to have an important impact on metal-based optical cavities, on-chip bright single photon sources and plasmon-based nanolasers.

DOI: 10.1103/PhysRevLett.114.193002 PACS numbers: 32.70.Cs, 42.50.Pq, 73.20.Mf

The study of single photon emission is of fundamental interest for research in cavity quantum electrodynamics (CQED) [1], single photon sources [2], and cavity-based lasing processes [3]. Based on the principle of the Purcell effect [4]—i.e., the modification of the density of states of the electromagnetic field to enhance the spontaneous emission rate—traditional CQED techniques have achieved considerable success in the control of single photon emission [5]. To meet the requirements of on-chip optics, various nanophotonic structures have been proposed to tailor the emission rates and the collection efficiency of radiated light [6–13]. Photonic crystals [6,7] can effectively enhance emission rates [8], and properly designed nanocavities can increase both the emission rates and the coupling efficiency to some specific modes [9]. Dielectric nanofibers with superior guided properties at the nanoscale have likewise been used to control emission rates and to achieve high extraction efficiency [10–13]. However, the maximum enhancement of emission rates in subwavelength dielectric structures can reach only several tens of γ_0, the spontaneous decay rate of the radiating dipole in vacuum.

To improve on that situation, plasmonic nanostructures with high optical density of states and strong light confinement were proposed [14–21]. On the one hand, the hot spots induced by localized surface plasmon polaritons (SPPs) in metallic nanoparticles enable high emission rates [14], which generally reach several hundreds of γ_0 [15,16]; on the other hand, plasmonic waveguide nanostructures have high extraction efficiency into the SPP channels [17–21]. However, in localized SPPs, it is difficult to collect the single photons generated, while in guided SPPs the total emission rate is relatively low, which limits their applicability.

Various hybrid plasmon nanostructures have been considered, both theoretically and experimentally, for overcoming these limitations and simultaneously achieving efficient emission and a high collection of single photons [22–26]. In metal-coated nanocylinder cavities [23], the collection efficiency is very high, but the total emission rates are only tens to hundreds times γ_0. Because of ultrastrong hot spots in the gap between the metallic nanoparticle and the layer, gap surface plasmon structures [27–30] can provide large spontaneous emission enhancement [22,26]. However, the nanoscale collection and guiding of the emitted photons necessary for on-chip optical circuits remain a problem.

In this Letter we demonstrate theoretically both efficient photon emission of a single dipole emitter and one-dimensional nanoscale guiding of single photons in gap plasmon structures that include a properly designed dielectric nanofiber. We focus primarily on a large SPP channel decay rate and demonstrate that it can be coupled effectively to phase-matched low-loss nanofibers, which can then be directly used in on-chip photonic devices. When compared with other theoretically proposed plasmonic resonant structures, such as plasmonic optical patch antennas [24], hybrid metallodielectric nanostructures [25], and metal-coated nanocylinder cavities [23], the proposed nanostructure combines the advantages of localized and propagating SPPs and, as a result, achieves ultrahigh total decay rates and large SPP channel decay rates.

The proposed system is schematically shown in Fig. 1. A silver nanorod is coupled to a gold nanofilm through a nanoscale gap, with a low-loss dielectric nanofiber positioned close to the nanorod above the nanofilm. In addition, a quantum emitter is inserted in the gap formed by the nanorod and the nanofilm. The role of the dielectric nanofiber is to transfer single plasmons to low-loss phase-matched nanofiber modes so that these

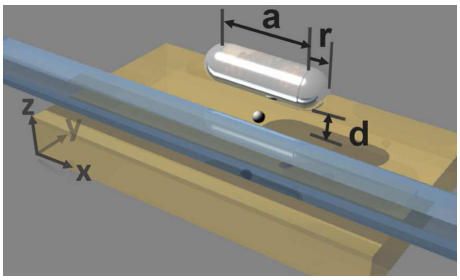

FIG. 1 (color online). Schematic diagram of Ag nanorod-coupled Au nanofilm gap plasmon system with a designed nanofiber.

guided single photons can be directly used in on-chip photonic circuits.

When the emitter is located at hot spots of the gap plasmons, we can achieve total decay rates that are 18–55 times larger and guided SPP channel decay rates that are 12–23 times larger than the corresponding values in metallic nanofilms alone, a result of combining the advantages of localized gap plasmons and guided SPPs. In particular, a maximum total decay rate of $5000\gamma_0$ and a SPP channel decay rate of $1500\gamma_0$ are achieved for a gap of 10 nm between the nanorod and the nanofilm. To reduce propagation losses, phase-matched low-loss nanofibers with an efficiency of 40% (with the decay rates of about $290\gamma_0$–$770\gamma_0$) are designed to guide these single plasmons along the direction of the nanorod orientation, which can be directly used in ultracompact bright single photon sources and on-chip plasmon-based nanolasers.

We consider the specific example that a silver nanorod (composed of a cylinder of length a and two semispheres with radius $r = 20$ nm) is placed at a distance d above a gold nanofilm, which supports the gap surface plasmons [27–30]. To provide better single photon emission directivity, a plasmonic nanorod with a well-defined orientation is preferred. The gold nanofilm with a thickness of 52 nm is sandwiched between a glass substrate with refractive index $n_g = 1.514$ and water with $n_w = 1.331$. It supports both long and short range SPPs, for which propagation constants and propagation lengths are given in the Supplemental Material [31]. Fifty-two nm is the cutoff thickness of long range SPPs at $\lambda = 680$ nm, which has an ultralong propagation length of 163 μm. The propagation length of a long range SPP decreases rapidly with increasing film thickness. Here the nanorod is too small to affect the SPPs of nanofilm. In particular, to achieve the largest enhancement of decay rates extracted into propagating SPPs, we selected the combination of Ag nanorod and Au nanofilm by optimizing the sets of Ag(Au) nanorod and Ag(Au) nanofilm. Furthermore, the low-loss phase-matched dielectric nanofiber is designed to guide single photons at long distance.

The quantum emitter inserted into the nanoscale gap formed by the nanorod and the nanofilm is simulated as an oscillating classical point dipole. Three-dimensional finite element simulations are performed using the COMSOL multiphysics software [34]. The model dimensions are $6 \times 3 \times 1.052$ μm^3, and a perfectly matched layer of 200 nm is introduced to minimize boundary reflections. The thicknesses of glass, gold, and water are 200, 52, and 800 nm, respectively, and the dielectric constant of metals is taken from the experimental data [35]. By enveloping the dipole in a 4 nm radius sphere and performing surface integrals over the Poynting vector $\mathbf{S}$ on the sphere, the radiated power of the dipole is obtained: $W_{\text{total}} = \int\int_{\Sigma} \mathbf{S} \bullet d\Sigma$. Thus, the normalized decay rate can be obtained from $\gamma_{\text{total}}/\gamma_0 = W_{\text{total}}/W_0$, where γ_0 and W_0 are the decay rate and the radiated power of the dipole in a vacuum [19,36].

The excited gap plasmons [27–30] can be separated into a localized part near the nanorod and a propagating part along the nanofilm. By assuming the propagating part is dominated by SPPs, total decay rates can be divided into three contributions: decay into the SPP channels γ_{SPP}, decay into nonradiative channels γ_{nr}, and radiative decay into free space γ_{r}. The nonradiative part $\gamma_{\text{nr}}/\gamma_0 = W_{\text{nr}}/W_0$ includes both the absorption inside the metallic nanorod and the absorption inside the metallic nanofilm below the nanorod (called the rod image), where the rod image is the concentration of charge induced by the nanorod and the emitter [29]. The decay rate into SPP channels is equal to the total decay rate minus the other channels' decay rates, i.e., $\gamma_{\text{SPP}} = \gamma_{\text{total}} - \gamma_{\text{nr}} - \gamma_{\text{r}}$. (The computation details are given in the Supplemental Material [31].) For our purposes, this is the most important part since single photons emitted into SPP channels can be guided and used in on-chip photonic devices. The quantum emitter (in the hot spots) oriented along the z axis is chosen because its total decay rate is several dozen times larger than that of x or y oriented dipole emitters.

We first explore the total decay rates γ_{total} and the SPP channel decay rates γ_{SPP} in the proposed gap plasmon nanostructures without nanofibers. When the dipole emitter is placed at the middle of the gap and the length a of the nanorod is varied, we find maximal values of both γ_{total} and γ_{SPP} at $a = 135$ nm [Fig. 2(a)]. This corresponds to the excitation of the quadrupolar gap plasmon, with the electric field pattern shown in the inset of Fig. 2(a). In contrast, when placing the dipole emitter at the left corner of the gap, maximal values of γ_{total} and γ_{SPP} occur at $a = 45$ and 138 nm; see Fig. 2(b). These correspond to both the dipolar [the inset of Fig. 2(b)] and the quadrupolar gap plasmons. In the hot spot at the middle of the gap [Fig. 2(a)], $\gamma_{\text{total}}/\gamma_0$ and $\gamma_{\text{SPP}}/\gamma_0$ can reach up to 5020 and 1582, which are 55 and 18 times larger than the values of the gold nanofilm alone (91- and 88-fold γ_0). While, in the hot spot at the left corner of the gap [Fig. 2(b)], the maximum $\gamma_{\text{total}}/\gamma_0$ and $\gamma_{\text{SPP}}/\gamma_0$ are 2957 and 839 for $a = 45$ nm, and 1602 and 472 for $a = 138$ nm. The excitation processes of both the

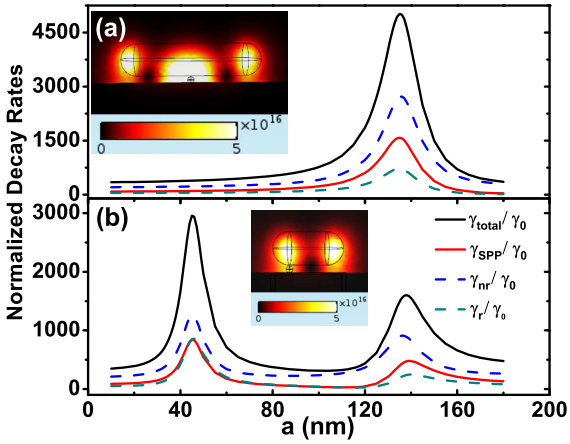

FIG. 2 (color online). Total normalized decay rates $\gamma_{\text{total}}/\gamma_0$ and SPP channel normalized decay rates $\gamma_{\text{SPP}}/\gamma_0$ for a dipole emitter (a) at the middle of the gap and (b) at the left corner of the gap, as a function of the length a of the nanorod. The gap between nanorod and nanofilm is 10 nm and $\lambda = 680$ nm. The insets in Figs. 2(a) and 2(b) are electric field patterns (on the tangent xz plane with the nanorod) of quadrupolar and dipolar gap plasmons.

dipolar and the quadrupolar gap mode in the evanescent wave are shown in the Supplemental Material [31], and the excitations by the dipole emitter are in the minivideo.

Though the emitted photons may be reflected several times between the nanorod and the nanofilm, the optical path difference is too small to affect their high-quality single photon property. Thus, the dip of the two-photon correlation $g^{(2)}(0)$ characteristic of a single photon should be very deep. Also, the linewidth of the dip of $g^{(2)}(0)$ and the emission spectrum should be very narrow, determined by the total decay rate. Because of the fast decay to the SPP channels, we ignore the possible strong coupling effect between the emitter and the nanorod. Moreover, the SPP channel decay rates are large enough to prevent the fluorescence quenching [37] near the metallic nanostructures.

The nonradiative decay rate coming from an intrinsic loss of metallic structures is very high. However, the valid part γ_{SPP} or the extraction into the nanofiber γ_{fiber} is large enough to be used in the on-chip quantum nanophotonics devices. To compensate for loss, more pump power is needed. For example, in the experiments on utilizing gap plasmon structures to enhance the emission rate [22,26], despite the existence of a large intrinsic loss, a high radiative emission rate is obtained as a useful part.

We now turn to the propagation direction and the emission angle for the collection of single plasmons. The model used here is adjusted to $10 \times 2 \times 1.052\ \mu\text{m}^3$ with the dipole placed 2 μm from one end. We explored the energy flux ratio as emitted single plasmons propagate along the x direction. In the analytical results [38], for a long range SPP with $k_x = 1.4283$, the energy flux ratio in the water and in the glass along the x direction is 90.23%:8.36%, while for the short range SPP with $k_x = 1.7043$, this ratio is 8.85%:88.15%. For the two cases discussed in Fig. 2, by comparing the results of the analysis with the COMSOL simulation, we obtain that most of the collected single plasmons are long range SPPs (see the Supplemental Material [31]). Additionally, by comparing the resonance lengths of a gold nanorod in an evanescent field of nanofilm with those in dipole excitation, a good agreement with 1–3 nm error is obtained. The error is the perturbations brought by excitations of short range SPPs and other tiny components, such as the radiation modes, quasicylindrical waves, and Norton waves [39–41].

From the electric field distribution of the quadrupolar gap mode ($a = 135$ nm) shown in Fig. 3(b), the emission angle is about 100° along the x direction. A smaller and more directional emission angle of about 60° along the negative x axis is achieved in Fig. 3(e), where the emitter is placed at the left corner of the gap and the dipolar gap mode is excited at $a = 45$ nm.

For practical applications of the emitted photons, previous researchers have used optical antennas to direct the single photons emitted from molecules [42] and metal-coated semiconductor nanostructures to collect the single photons from an InAs quantum dot [43,44]. Here, phase-matched low-loss nanofibers are designed to effectively guide these single photons, and the eigenmodes of nanofibers are obtained by the mode analysis study of the COMSOL software.

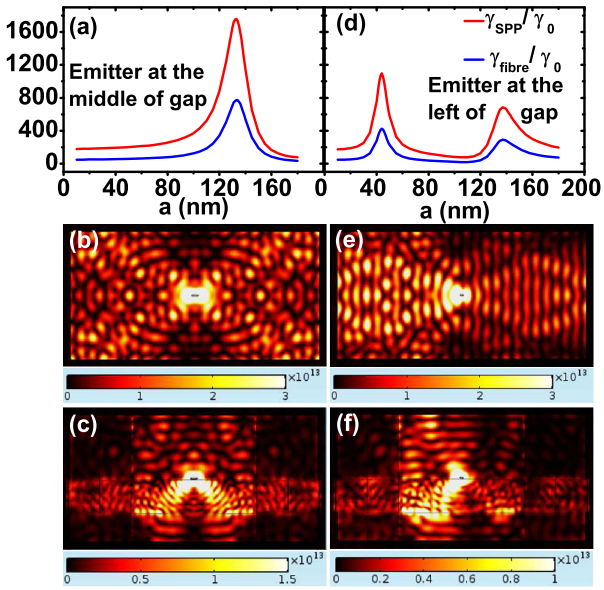

FIG. 3 (color online). $\gamma_{\text{SPP}}/\gamma_0$ and $\gamma_{\text{fiber}}/\gamma_0$ for the dipole emitter (a) at the middle of the gap and (d) at the left corner of the gap with a varying of the length a of the Ag nanorod. Electric field patterns of the $z = 282$ nm plane (in water 30 nm above the nanofilm) for $a = 135$ nm (b) without and (c) with the nanofiber for a quadrupolar gap mode with a size of $6 \times 3\ \mu\text{m}^2$, and electric field patterns of the $z = 282$ nm plane for $a = 45$ nm (e) without and (f) with the nanofiber for the dipolar gap mode.

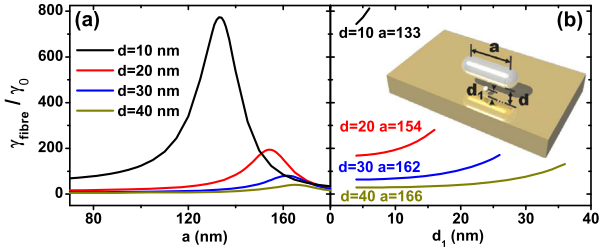

FIG. 4 (color online). Changes of $\gamma_{\text{fiber}}/\gamma_0$ when varying the distances (a) d and (b) d_1. In (a), the emitter is fixed at $d_1 = d/2$ under the nanorod. The maximum $\gamma_{\text{fiber}}/\gamma_0$ appears when the emitter is nearest the nanorod because of the existence of hot spots.

Nanofiber extraction decay rates γ_{fiber} can achieve over $500\gamma_0$ with optimized geometrical parameters, as the nanofiber refractive index changes from 2.0 to 3.5, corresponding to various semiconductor compounds and glasses, such as GaN, Si_3N_4, etc. γ_{fiber} is calculated by performing surface integrals over the Poynting vector $\mathbf{S}_x$ on the fiber cross section 1.5 μm away from the emitter, and the gold film dimension in the xy plane is changed to 3×3 μm^2 to avoid interactions between the nanofiber and the nanofilm. Specifically, we study the case of Si_3N_4 and obtain the maximal γ_{fiber} of $774\gamma_0$. At $\lambda = 680$ nm, the refractive index of Si_3N_4 is $n = 2.4631$ [45]. The Si_3N_4 nanofiber with an xz section dimension of 800×640 nm^2 is designed to be phase matched with both SPPs of the gold nanofilms, which are placed at a distance of 10 nm from the nanorod surface and 10 nm from the nanofilm. From electric field patterns with nanofibers shown in Figs. 3(c) and 3(f), it is evident that photons emitted into the SPP channels can efficiently couple into the nanofiber with a $\gamma_{\text{fiber}}/\gamma_0$ of 290–770 [Figs. 3(a) and 3(d)]. This demonstrates that the efficient one-dimensional nanoscale guiding of single photons can be achieved.

When the distance d between the nanorod and the nanofilm is varied from 10 to 40 nm and the dipole emitter is fixed at $d_1 = d/2$ under the nanorod, we obtain γ_{fiber} in the range of $40\gamma_0$–$770\gamma_0$. As shown in Fig. 4(a), as d increases, γ_{fiber} decreases dramatically because of a weaker coupling between the nanorod and the nanofilm. The maximum γ_{fiber} moves to the longer nanorod due to the shift of the quadrupolar gap plasmons. Then, when the distance between the nanorod and the nanofilm is fixed, while the distance d_1 between the dipole emitter and the nanofilm is varied, the maximum γ_{fiber} appears when the emitter is nearest the nanorod due to the existence of hot spots.

Using currently available nanotechnologies, the nanoparticle-coupled nanofilm plasmon structures have been fabricated [25,26,30,46] where the size of the nanorod and the nanofilm and the gap distance can be accurately controlled. Inserting a single upright emitter into the nanoscale gap is challenging, but it can be done. For example, by performing single molecule studies, terrylene molecules in a spin-coated ultrathin crystalline film of p-terphenyl can be aligned [47]. For directional single photon emission, an emitter with a normal orientation can be inserted into a planar dielectric antenna and can be efficiently excited via a total internal reflection of the p-polarized incident light through the microscope objective [48]. Moreover, the phase-matched nanofiber for guiding the SPPs has been fabricated by various methods including chemical synthesis and laser ablation [49,50]. This strongly suggests that, using the above techniques, it will be feasible to experimentally realize our design in the near future.

In summary, we have designed nanorod-coupled nanofilm gap plasmon nanostructures with low-loss nanofiber, and we have obtained both ultralarge total decay rates and large extraction decay rates into the nanofiber when the dipole emitter is placed in hot spots of the gap plasmons. The proposed nanostructures will generate fundamental research interest in CQED [1] and will lead to possible applications in on-chip single photon sources and plasmon-based nanolasers. In ordinary plasmonic nanocavities, while the optical mode volume is small, the large intrinsic losses prevent the achievement of the strong coupling region [5]. However, if gap plasmons are combined with other low-loss photonic nanostructures, broader coupling regions may be accessible. The nanoscale guiding of high rate single photons also makes our structures promising candidates for on-chip single photon sources [2] since it significantly reduces the losses of propagating single surface plasmons. Finally, a nanorod-nanofilm gap cavity enabling high rate emission shows good confinement properties, and a low-loss nanofiber provides efficient out guiding; thus, a high-quality on-chip plasmon-based nanolaser may very possibly be realized by putting gain material in this plasmonic cavity [51,52], thereby realizing an important component of on-chip photonic circuits [53].

We thank P. Meystre, X. F. Ren, and X. W. Chen for the useful discussions. This work was supported by the National Key Basic Research Program under Grant No. 2013CB328700, and by the National Natural Science Foundation of China under Grants No. 11374025, No. 91121018, No. 91221304, and No. 11121091.

*ygu@pku.edu.cn

[1] P. R. Berman, in *Cavity Quantum Electrodynamics* (Academic Press, Boston, 1994).
[2] B. Lounis and M. Orrit, Single-photon sources, Rep. Prog. Phys. **68**, 1129 (2005).
[3] H. Yokoyama, Physics and device applications of optical microcavities, Science **256**, 66 (1992).
[4] E. M. Purcell, Spontaneous emission probabilities at radio frequencies, Phys. Rev. **69**, 681 (1946).
[5] K. J. Vahala, Optical microcavities, Nature (London) **424**, 839 (2003).

[6] E. Yablonovitch, Inhibited Spontaneous Emission in Solid-State Physics and Electronics, Phys. Rev. Lett. **58**, 2059 (1987).
[7] M. D. Leistikow, A. P. Mosk, E. Yeganegi, S. R. Huisman, A. Lagendijk, and W. L. Vos, Inhibited Spontaneous Emission of Quantum Dots Observed in a 3D Photonic Band Gap, Phys. Rev. Lett. **107**, 193903 (2011).
[8] P. Lodahl, A. F. van Driel, I. S. Nikolaev, A. Irman, K. Overgaag, D. Vanmaekelbergh, and W. L. Vos, Controlling the dynamics of spontaneous emission from quantum dots by photonic crystals, Nature (London) **430**, 654 (2004).
[9] W.-H. Chang, W.-Y. Chen, H.-S. Chang, T.-P. Hsieh, J.-I. Chyi, and T.-M. Hsu, Efficient Single-Photon Sources Based on Low-Density Quantum Dots in Photonic-Crystal Nanocavities, Phys. Rev. Lett. **96**, 117401 (2006).
[10] V. V. Klimov and M. Ducloy, Spontaneous emission rate of an excited atom placed near a nanofiber, Phys. Rev. A **69**, 013812 (2004).
[11] J. Bleuse, J. Claudon, M. Creasey, N. S. Malik, J-M. Gérard, I. Maksymov, J. P. Hugonin, and P. Lalanne, Inhibition, Enhancement, and Control of Spontaneous Emission in Photonic Nanowires, Phys. Rev. Lett. **106**, 103601 (2011).
[12] R. Yalla, F. Le Kien, M. Morinaga, and K. Hakuta, Efficient Channeling of Fluorescence Photons from Single Quantum Dots into Guided Modes of Optical Nanofiber, Phys. Rev. Lett. **109**, 063602 (2012).
[13] J. Claudon, J. Bleuse, N. S. Malik, M. Bazin, P. Jaffrennou, N. Gregersen, C. Sauvan, P. Lalanne, and J.-M. Gérard, A highly efficient single-photon source based on a quantum dot in a photonic nanowire, Nat. Photonics **4**, 174 (2010).
[14] R. Ruppin, Decay of an excited molecule near a small metal sphere, J. Chem. Phys. **76**, 1681 (1982).
[15] C. Sauvan, J. P. Hugonin, I. S. Maksymov, and P. Lalanne, Theory of the Spontaneous Optical Emission of Nanosize Photonic and Plasmon Resonators, Phys. Rev. Lett. **110**, 237401(2013).
[16] J-W. Liaw, Analysis of a bowtie nanoantenna for the enhancement of spontaneous emission, IEEE J. Sel. Top. Quantum Electron. **14**, 1441(2008).
[17] R. R. Chance, A. Prock, and R. Silbey, Comments on the classical theory of energy transfer, J. Chem. Phys. **62**, 2245 (1975).
[18] Y.-T. Chen, T. R. Nielsen, N. Gregersen, P. Lodahl, and J. Mørk, Finite-element modeling of spontaneous emission of a quantum emitter at nanoscale proximity to plasmonic waveguides, Phys. Rev. B **81**, 125431 (2010).
[19] Y. C. Jun, R. D. Kekatpure, J. S. White, and M. L. Brongersma, Nonresonant enhancement of spontaneous emission in metal-dielectric-metal plasmon waveguide structures, Phys. Rev. B **78**, 153111 (2008).
[20] A. V. Akimov, A. Mukherjee, C. L. Yu, D. E. Chang, A. S. Zibrov, P. R. Hemmer, H. Park, and M. D. Lukin, Generation of single optical plasmons in metallic nanowires coupled to quantum dots, Nature (London) **450**, 402 (2007).
[21] D. E. Chang, A. S. Sørensen, P. R. Hemmer, and M. D. Lukin, Quantum Optics with Surface Plasmon, Phys. Rev. Lett. **97**, 053002 (2006).
[22] K. J. Russell, T.-L. Liu, S. Cui, and E. L. Hu, Large spontaneous emission enhancement in plasmonic nanocavities, Nat. Photonics **6**, 459 (2012).
[23] I. S. Maksymov, M. Besbes, J. P. Hugonin, J. Yang, A. Beveratos, I. Sagnes, I. Robert-Philip, and P. Lalanne, Metal-Coated Nanocylinder Cavity for Broadband Nonclassical Light Emission, Phys. Rev. Lett. **105**, 180502 (2010).
[24] R. Esteban, T. V. Teperik, and J. J. Greffet, Optical Patch Antennas for Single Photon Emission Using Surface Plasmon Resonances, Phys. Rev. Lett. **104**, 026802 (2010).
[25] X.-W. Chen, M. Agio, and V. Sandoghdar, Metallodielectric Hybrid Antennas for Ultrastrong Enhancement of Spontaneous Emission, Phys. Rev. Lett. **108**, 233001 (2012).
[26] G. M. Akselrod, C. Argyropoulos, T. B. Hoang, C. Ciracì, C. Fang, J. Huang, D. R. Smith, and M. H. Mikkelsen, Probing the mechanisms of large Purcell enhancement in plasmonic nanoantennas, Nat. Photonics **8**, 835 (2014).
[27] G. Lévêque and O. J. F. Martin, Optival interactions in a plasmonic particle coupled to a metallic film, Opt. Express **14**, 9971 (2006).
[28] F. Le, N. Z. Lwin, J. M. Steele, M. Käll, N. J. Halas, and P. Nordlander, Plasmons in the metallic nanoparticle-film system as a tunable impurity problem, Nano Lett. **5**, 2009 (2005).
[29] J. J. Mock, R. T. Hill, A. Degiron, S. Zauscher, A. Chilkoti, and D. R. Smith, Distance-dependent plasmon resonant coupling between a gold nanoparticle and gold film, Nano Lett. **8**, 2245 (2008).
[30] J. B. Lassiter, F. McGuire, J. J. Mock, C. Ciracì, R. T. Hill, B. J. Wiley, A. Chilkoti, and D. R. Smith, Plasmonic waveguide modes of film-coupled metallic nanocubes, Nano Lett. **13**, 5866 (2013).
[31] See Supplemental Material at http://link.aps.org/supplemental/10.1103/PhysRevLett.114.193002, which includes Refs. [32,33], for SPPs of Au nanofilm, the excitation of a gap surface plasmon in an evanscent wave, the fraction of a long range SPP, and a video displaying the excitation processes of gap plasmons by a dipole emitter.
[32] F. Pigeon, I. F. Salakhutdinov, and A. V. Tishchenko, Identity of long-range surface plasmons along asymmetric structures and their potential for refractometric sensors, J. Appl. Phys. **90**, 852 (2001).
[33] H. Raether, *Surface Plasmons on Smooth and Rough Surfaces and on Gratings* (Springer-Verlag, Heidelberg, 1988).
[34] X.-N. Shan, I. Díez-Pérez, L.-J. Wang, P. Wiktor, Y. Gu, L.-H. Zhang, W. Wang, J. Lu, S.-P. Wang, Q.-H. Gong, J.-H. Li, and N.-J. Tao, Imaging the electrocatalytic activity of single nanoparticles, Nat. Nanotechnol. **7**, 668 (2012).
[35] D. L. Windt, W. C. Cash, Jr., M. Scott, P. Arendt, B. Newnam, R. F. Fisher, and A. B. Swartzlander, Optical constants for thin films of Ti, Zr, Nb, Mo, Ru, Rh, Pd, Ag, Hf, Ta, W, Re, Ir, Os, Pt, and Au from 24 Å to 1216 Å, Appl. Opt. **27**, 246 (1988).
[36] M.-Z. Liu, T. W. Lee, S. K. Gray, P. Guyot-Sionnest, and M. Pelton, Excitation of Dark Plasmons in Metal Nanoparticles by a Localized Emitter, Phys. Rev. Lett. **102**, 107401 (2009).
[37] P. Anger, P. Bharadwaj, and L. Novotny, Enhancement and Quenching of Single-Molecule Fluorescence, Phys. Rev. Lett. **96**,113002 (2006).

[38] L.-J. Wang, Y. Gu, X.-Y. Hu, and Q.-H. Gong, Long-range surface plasmon polariton modes with a large field localized in a nanoscale gap, Appl. Phys. B **104**, 919 (2011).

[39] J. J. Burke and G. I. Stegeman, Surface-polariton-like waves guided by thin, lossy metal films, Phys. Rev. B **33**, 5186 (1986).

[40] P. Lalanne, J. P. Hugonin, H. T. Liu, and B. Wang, A microscopic view of the electromagnetic properties of sub-λ metallic surfaces, Surf. Sci. Rep. **64**, 453 (2009).

[41] A. Yu. Nikitin, S. G. Rodrigo, F. J. García-Vidal, and L. Martín-Moreno, In the diffraction shadow: Norton waves versus surface plasmon polaritons in the optical region, New J. Phys. **11**, 123020 (2009).

[42] T. H. Taminiau, F. D. Stefani, F. B. Segerink, and N. F. Van Hulst, Optical antennas direct single-molecule emission, Nat. Photonics **2**, 234 (2008).

[43] X. Liu, T. Asano, S. Odashima, H. Nakajima, H. Kumano, and I. Suemune, Bright single-photon source based on an InAs quantum dot in a silver-embedded nanocone structure, Appl. Phys. Lett. **102**, 131114 (2013).

[44] I. Suemune, H. Nakajima, X.-M. Liu, S. Odashima, T. Asano, H. Iijima, J.-H. Huh, Y. Idutsu, H. Sasakura, and H. Kumano, Metal-coated semiconductor nanostructures and simulation of photon extraction and coupling to optical fibers for a solid-state single-photon source, Nanotechnology **24**, 455205 (2013).

[45] J. Kischkat, S. Peters, B. Gruska, M. Semtsiv, M. Chashnikova, M. Klinkmüller, O. Fedosenko, S. Maachulik, A. Aleksandrova, G. Monastyrskyi, Y. Flores, and W. T. Masselink, Mid-infrared optical properties of thin films of aluminum oxide, titanium dioxide, silicon dioxide, aluminum nitride, and silicon nitride, Appl. Opt. **51**, 6789 (2012).

[46] D. O. Sigle, J. T. Hugall, S. Ithurria, B. Dubertret, and J. J. Baumberg, Probing Confined Phonon Modes in Individual CdSe Nanoplatelets Using Surface-Enhanced Raman Scattering, Phys. Rev. Lett. **113**, 087402 (2014).

[47] R. J. Pfab, J. Zimmermann, C. Hettich, I. Gerhardt, A. Renn, and V. Sandoghdar, Aligned terrylene molecules in a spin-coated ultrathin crystalline film of *p*-terphenyl, Chem. Phys. Lett. **387**, 490 (2004).

[48] K. G. Lee, X. W. Chen, H. Eghlidi, P. Kukura, R. Lettow, A. Renn, V. Sandoghdar, and S. Götzinger, A planar dielectric antenna for directional single-photon emission and near-unity collection efficiency, Nat. Photonics **5**, 166 (2011).

[49] L. Brus, Chemical approaches to semiconductor nanocrystals, J. Phys. Chem. Solids **59**, 459 (1998).

[50] A. M. Morales and C. M. Lieber, A laser ablation method for the synthesis of crystalline semiconductor nanowires, Science **279**, 208 (1998).

[51] P. Berini and I. De Leon, Surface plasmon-polariton amplifiers and lasers, Nat. Photonics **6**, 16 (2012).

[52] M. A. Noginov, G. Zhu, A. M. Belgrave, R. Bakker, V. M. Shalaev, E. E. Narimanov, S. Stout, E. Herz, T. Suteewong, and U. Wiesner, Demonstration of a spaser-based nanolaser, Nature (London) **460**, 1110 (2009).

[53] E. Ozbay, Plasmonics: Merging photonics and electronics at nanoscale dimensions, Science **311**, 189 (2006).